PNAS RESEARCH ARTICLE | BIOPHYSICS AND COMPUTATIONAL BIOLOGY

Elastin recoil is driven by the hydrophobic effect

Nour M. Jamhawi[a], Ronald L. Koder[b,c], and Richard J. Wittebort[a,1]

Edited by Robert Griffin, Massachusetts Institute of Technology, Cambridge, MA; received March 28, 2023; accepted February 1, 2024

Elastin is an extracellular matrix material found in all vertebrates. Its reversible elasticity, robustness, and low stiffness are essential for the function of arteries, lungs, and skin. It is among the most resilient elastic materials known: During a human lifetime, arterial elastin undergoes in excess of 2×10^9 stretching/contracting cycles without replacement, and slow oxidative hardening has been identified as a limiting factor on human lifespan. For over 50 y, the mechanism of entropic recoil has been controversial. Herein, we report a combined NMR and thermomechanical study that establishes the hydrophobic effect as the primary driver of elastin function. Water ordering at the solvent:protein interface was observed as a function of stretch using double quantum ^{2}H NMR, and the most extensive thermodynamic analysis performed to date was obtained by measuring elastin length and volume as a function of force and temperature in normal water, heavy water and with cosolvents. When stretched, elastin's heat capacity increases, water is ordered proportional to the degree of stretching, the internal energy decreases, and heat is released in excess of the work performed. These properties show that recoil in elastin under physiological conditions is primarily driven by the hydrophobic effect rather than by configurational entropy as is the case for rubber. Consistent with this conclusion are decreases in the thermodynamic signatures when cosolvents that alter the hydrophobic effect are introduced. We propose that hydrophobic effect-driven recoil, as opposed to a configurational entropy mechanism where hardening from crystallization can occur, is the origin of elastin's unusual resilience.

elastin | recoil | NMR | thermodynamics

Significance

Elastin, found in tissues that require reversible elasticity, has low stiffness and great resiliency. It is a self-assembled material that has been a target for regenerative medicine. However, the basis for its elasticity has been controversial for more than 50 y. Formed from a hydrophobic protein with an equivalent mass of water, the controversy is whether recoil is driven by entropy gain of the protein and/or the water. We demonstrate that matrix water is progressively ordered upon stretching and that the thermodynamics of elastin recoil are those of the hydrophobic effect and different from those of rubber. We conclude that recoil is primarily driven by the hydrophobic effect and suggest that this accounts for elastin's low stiffness and high resilience.

Although elastin has been identified as one of the limiting factors on human lifespan (1), its molecular mechanism of entropic recoil is not well understood and has been a source of controversy for over 50 y (2–12). A widely accepted hypothesis is that elastin is like rubber and an increase in the polymer's configurational entropy drives recoil (2, 3, 13). Unlike rubber, elastin gains elasticity only when swollen with an approximately equal mass of water (14) and its physiological function requires different mechanical properties: First, elastin recoil is fully reversible on the timescale of a heartbeat. This enables the elastic energy stored in arteries when the heart contracts to be fully recovered when the heart relaxes between beats. Second, elastin is highly compliant, with a Young's modulus (~0.4 MPa) that is an order of magnitude less than a typical rubber (~10 MPa) (15). Third, elastin is far more robust than rubber (16), undergoing more than 2×10^9 expansion/contraction cycles without appreciably lengthening during a normal human lifespan and failure of any of these properties results in hypertension which in turn causes vascular calcification, ventricular hypertrophy, renal dysfunction, and stroke.

The elastic matrix is formed when tropoelastin, one of the most hydrophobic proteins found in nature, is exported to the extracellular matrix and undergoes a liquid–liquid phase separation followed by enzymatic cross-linking (17, 18). Tropoelastin is organized in alternating proline-rich hydrophobic domains and alanine-rich crosslinking domains (Fig. 1*A*) (19). In 1970, Weis-Fogh (20) found that the amount of heat released when elastin is stretched is in large excess over the applied work (ΔG) and concluded that, unlike rubber (21, 22), elastin's internal energy decreases when stretched (4, 9, 23). It was hypothesized that the solvent-exposed surface area of hydrophobic droplets increases when deformed and ordering of water at the hydrophobic surface of elastin droplets is increased, i.e., spontaneous recoil is driven by the hydrophobic effect. Flory and Hoeve rejected the droplet model (2) in favor of a rubber-like network and pointed out that the thermodynamic analysis of Weis-Fogh (4) had neglected the contribution to the change in internal energy from a volume change that could occur when the sample is stretched, and they found that elastin's volume and internal energy are constant when stretched in aqueous glycol (3:7) or 30% PEG (polyethylene glycol). They concluded that elastin is like rubber, i.e., configurational entropy of the polymer drives recoil (2, 3). However, their analysis neglected the effect of glycol or PEG on water:protein interactions (24, 25) and it was subsequently reported (9) that elastin's volume is constant when stretched in water.

Author affiliations: [a]Department of Chemistry, University of Louisville, Louisville, KY 40292; [b]Department of Physics, The City College of New York, New York, NY 10031; and [c]Graduate Programs of Physics, Chemistry, Biology and Biochemistry, The Graduate Center City University of New York (CUNY), New York, NY 10016

Author contributions: N.M.J. and R.J.W. designed research; N.M.J. and R.J.W. performed research; N.M.J., R.L.K., and R.J.W. analyzed data; and N.M.J., R.L.K., and R.J.W. wrote the paper.

The authors declare no competing interest.

This article is a PNAS Direct Submission.

[1]To whom correspondence may be addressed. Email: dick.wittebort@louisville.edu.

This article contains supporting information online at https://www.pnas.org/lookup/suppl/doi:10.1073/pnas.2304009121/-/DCSupplemental.

Published March 5, 2024.

In this report, stretch-induced ordering of water (^2H_2O) in the elastin matrix was quantified using double quantum (2Q) filtered ^2H NMR, (26, 27) and a complete thermodynamic study of elastin's mechanical properties was obtained. The NMR experiment uses the property that isotropic molecular tumbling in bulk water (^2H_2O) averages the ^2H quadrupole coupling to zero whereas tumbling of water at a hydrophobic surface is anisotropic and the coupling is non-zero. Using the methods of multiple quantum spectroscopy, the bulk water signal is eliminated from detection and only the 2Q signal from ordered water is observed as the sample is stretched (28). We have determined elastin's thermodynamic properties with a custom-made thermo-mechanical apparatus. The length and volume of a purified elastin sample were measured with a high-resolution camera as a function of applied force and temperature (from 3 °C to 55 °C) in several aqueous solvents from which virial equations of state were constructed and the relevant thermodynamic properties, ΔG, ΔS, ΔH, ΔU, and ΔC_p, were calculated as functions of temperature and strain. Of particular interest are the dependencies of the heat capacity, enthalpy, and entropy with temperature and strain. When water molecules contact a hydrophobic surface, they are weakly ordered (29), the H-bond angle becomes more ideal and the H-bond length decreases (30). Consequently, entropy is lower and heat is released. As the temperature is increased, water is less ordered and the H-bond lengthens, i.e., ΔS and ΔH both increase (become less negative) resulting in a comparatively small change in ΔG (29), known as entropy–enthalpy compensation. With reduced heat loss, the heat capacity increases (31).

Results

Reversibility and the Equation of State. Fig. 1*A* depicts the domain structure of bovine elastin (747 residues) and Fig. 1*B* depicts a scanning electron micrograph demonstrating that the fibrous structure of natural elastin has been preserved in the purification procedure used here (32). A requirement in our thermodynamic analysis is reversibility of the length following changes in the applied force or temperature. Fig. 1 *C* and *D* show

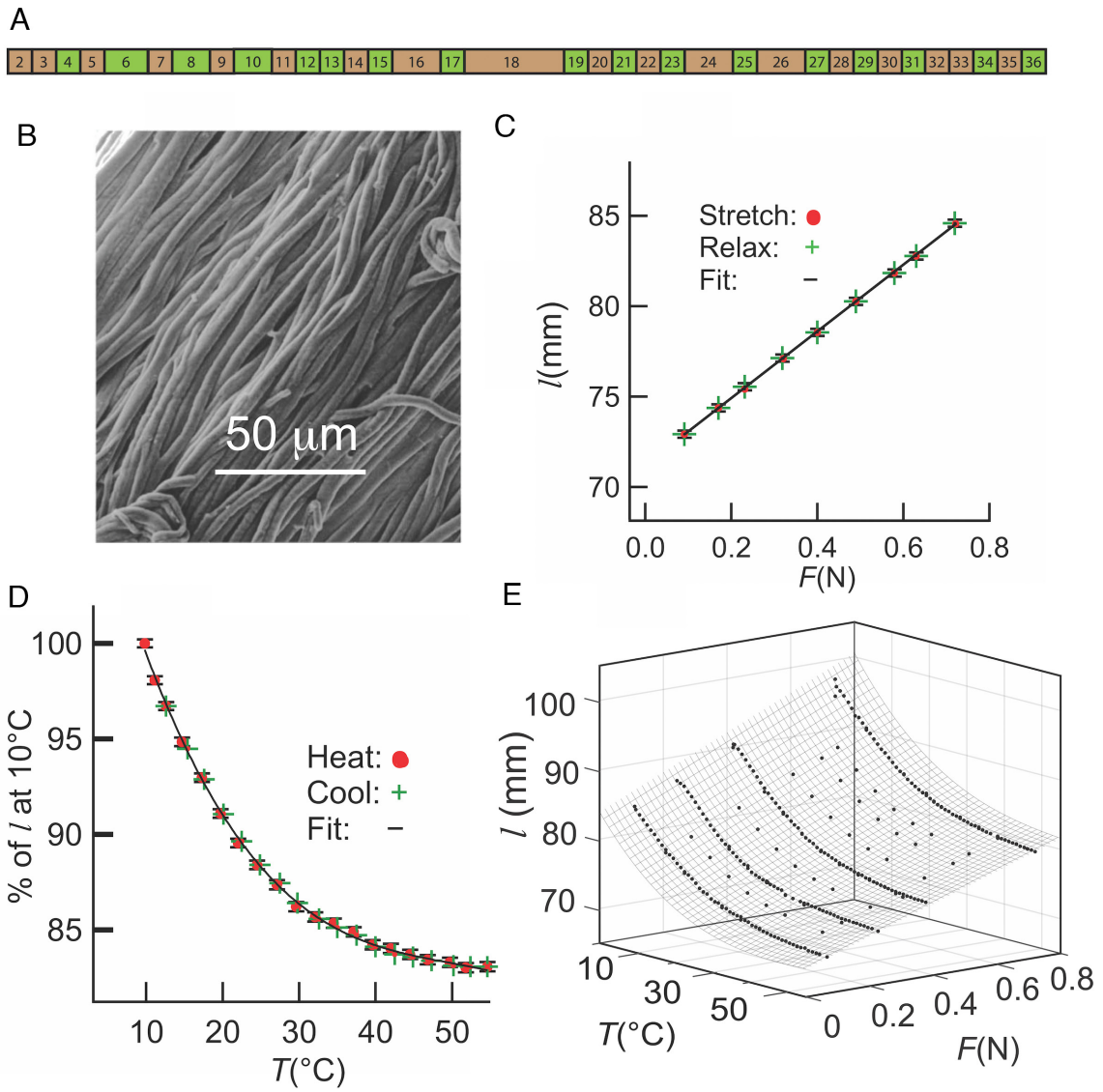

Fig. 1. (*A*) Domain architecture of bovine elastin. Brown rectangles represent hydrophobic domains and green rectangles represent crosslinking domains. (*B*) SEM of purified bovine elastin showing the uniform fibrous structure found in natural elastin. (*C*) Reversibility of the fiber length from two stretch and contract cycles. The fit to two cycles (line) is linear. (*D*) Reversibility from heating and cooling. The fit (line) is a polynomial 3rd-order in *T*. (*E*) Surface plot, *l(F, T),* obtained by combining data from multiple *l* vs. *F* and *l* vs. *T* experiments. The fit (lines) is a polynomial 1st-order in *F* and 3rd-order in *T*.

that elastin's length subjected to stretch/contract and heat/cool cycling is, as expected, fully reversible on the time scales of ~5 min for length changes and 3 to 5 min for temperature changes. From 3 °C to 55 °C, the decrease in length, l, is non-linear and reaches a temperature-independent length above ~50 °C (Fig. 1*D*). The variation of l with force, F, is linear as previously reported (9). The $l(F, T)$ surface (Fig. 1*E*), was obtained by combining multiple $l(F)$ and $l(T)$ data sets and fitting 308 data points (elastin in water) to a virial equation of state (Eq. **8**). The rmsd of 0.26 mm is comparable to the estimated accuracy of the length measurements. Fit parameters for elastin in water and in other solvents are listed in *SI Appendix*, Table S1. The equation of state (Eq. **8**) is conveniently expressed in the form of Hooke's law (Eq. **11**) with relaxed length, l_{rlx} (Eq. **9**) and force constant, k_H (Eq. **10**).

Elastin's Mechanical and Thermodynamic Properties in Pure Water and Comparison to Natural Rubber. The thermo-mechanical parameters obtained from purified elastin in water at 10 °C, 35 °C, and 45 °C are summarized in Fig. 2. Solid lines were calculated using Eqs. **9**–**17** and the virial equation coefficients in *SI Appendix*, Table S1. Error bars, shown at regular intervals along the solid lines, are SD of distributions of the thermodynamic property obtained by propagating uncertainties in the virial coefficients into SD of each property (33) as described in the *Materials and Methods* and used throughout this manuscript. So that data from different experiments could be directly compared, a single sample with randomly oriented fibers was used for all experiments and its integrity was confirmed by the reproducibility of the length vs. temperature curves obtained following experiments in different solvents, *SI Appendix*, Fig. S6. Samples with different fiber orientations potentially yield somewhat different results, however, the Young's modulus, 0.4 MPa at 37 °C (Fig. 2*A*), is in good agreement with the value of 0.45 MPa previously determined from unpurified, single-fiber samples (23). As temperature is raised, the change in E results from a force constant that increases linearly and a relaxed length that decreases in a non-linear way (Fig. 2*B*) indicating increased attractive forces in the elastin matrix. The relaxed length reaches a constant value at temperatures above ~50 °C (Fig. 2*B*).

Elastin and rubber tension (force per unit area) measured at constant T and P can be directly compared. Tension, f, in elastin is less than that of rubber and varies linearly with strain (Fig. 2*C*). With Eq. **7**, f can be separated into entropic and enthalpic components ($f = f_S + f_H$) (13, 23). Ratios of f and f_S were calculated for elastin using *SI Appendix*, Eq. **S4** with the virial coefficients listed in *SI Appendix*, Table S1 for elastin and values of f and f_S from the data of Shen et al. (21) for rubber. The ratios of f_S/f for elastin at 30 °C and 50 °C are depicted as a functions of strain and compared to rubber at 30 °C (Fig. 2*D*) (21). The horizontal line, $f_S/f = 1$, represents an ideal elastomer in which case the force is entirely entropic. At 30 °C and strains greater than 20%, rubber is approximately ideal ($f_S/f \sim 0.8$), whereas elastin is far from ideal at all strains ($f_S/f > 4$). When the temperature of elastin is raised to 50 °C, the entropic contribution to the total tension approaches that observed in rubber. Because the entropic tension is large compared to the net tension at physiological temperatures, the entropic and enthalpic tensions are opposed in elastin and the magnitude of the enthalpic tension, $f - f_S$, is almost as large as the entropic component and decreases in parallel with f_S as the temperature is increased.

Elastin's thermodynamic properties as functions of strain and temperature are depicted in Fig. 2 *E* and *F*. The expressions used to obtain ΔG, ΔH, ΔS, and ΔCp from the virial equation of state, are derived in the *Materials and Methods* section and apply to an open system at constant temperature and pressure that is in equilibrium with the surrounding water. The thermodynamic parameters determined in this way are for the entire system and change

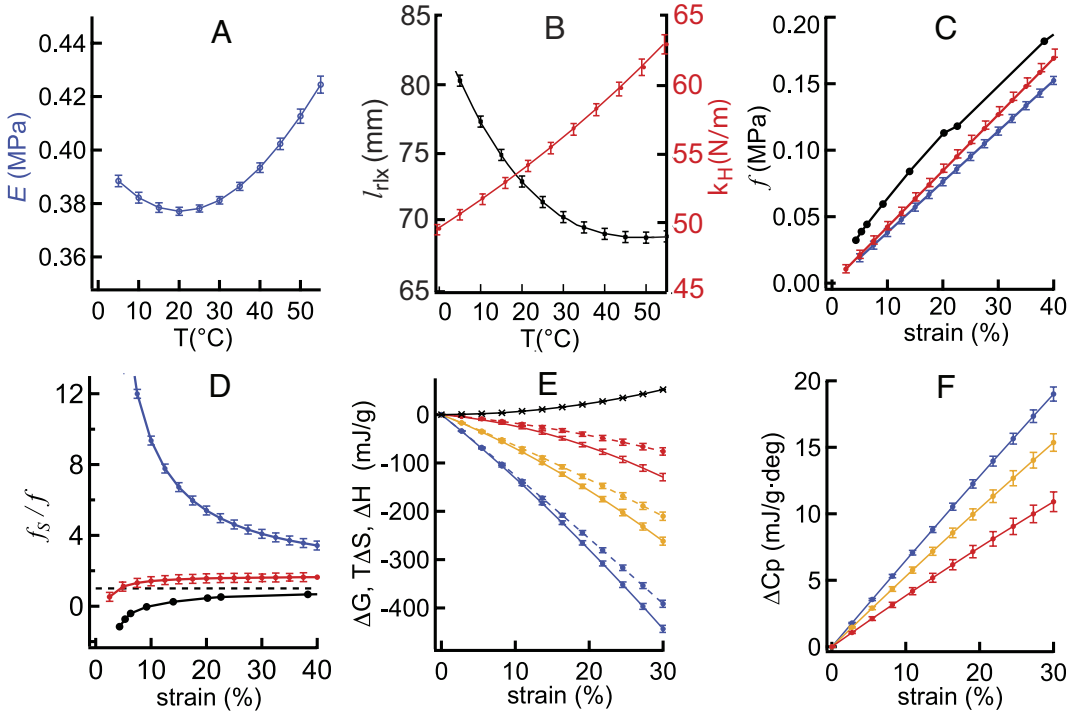

Fig. 2. Temperature dependence of elastin's mechanical and thermodynamic properties. (*A*) Young's modulus, (*B*) the relaxed length, l_{rlx} (black), and the force constant, k_H (red). (*C*) Tension, f, as a function of strain for elastin at 30 °C (blue), elastin at 50 °C red and rubber at 30 °C (black). (*D*) Ratio of the entropic tension to the total tension, f_S/f, as a function of strain for elastin at 30 °C (blue), elastin at 50 °C (red), and rubber at 30 °C (black). (*E*) Elastin ΔG (black), ΔH (···) and $T\Delta S$ (–) vs. strain at 10 °C (blue), 25 °C (yellow), and 45 °C (red). ΔG values at 10 °C, 25 °C, and 45 °C overlap. (*F*) Elastin ΔC_p vs. strain at 10 °C (blue), 25 °C (yellow), and 45 °C (red).

as the temperature and sample length are varied. Importantly, the heat to work ratios, $\Delta H/\Delta G$, determined at 23 °C using our method when elastin is stretched to strains of 10%, 20%, and 30% are −23 ± 0.3, −11.9 ± 0.3, and −8.1 ± 0.2, respectively, which are in agreement with values previously determined calorimetrically (9).

Elastin's thermodynamic properties are fully consistent with the conclusion that stretch increases the exposure of elastin's predominantly hydrophobic residues to water and this contributes to the net thermodynamic force that drives recoil: when elastin is stretched from the relaxed state, ΔH and $T\Delta S$ are negative at all values of strain and temperature and their small net difference, ΔG, gives elastin its physiologically important property of high compliance (low Young's modulus). The magnitudes of ΔH and $T\Delta S$ decrease substantially as the temperature is raised while ΔG is nearly independent of temperature. At temperatures below 45 °C, spontaneous recoil in elastin is endothermic and entropy driven with a free energy change that is less than the heat liberated. Elastin's heat capacity (Fig. 2*F*) has not been previously determined and we find that ΔCp increases when strain is applied. The pattern of changes in ΔG, ΔH, and $T\Delta S$ (Fig. 2*E*) and the increase in heat capacity (Fig. 2*D*) are all characteristic features of the transfer of hydrophobic substances into an aqueous environment (29, 30, 34). The decrease in the amount of ordered water and its concomitant decrease in volume are expected consequences of the hydrophobic effect.

Volume Expansion and Water Uptake is Small when Elastin is Stretched. Because heat is in large excess of the work performed when stretched, it was concluded that, unlike rubber, elastin's internal energy decreases when stretched (4, 9). McCrum et al., in a series of papers, pointed out that this conclusion neglected a change in volume that could occur when elastin is stretched and proposed that the release of heat from water uptake associated with an increased volume could account for the large release of heat when elastin is stretched (2, 5–7). However, it was subsequently reported that the increase in elastin's volume when extended by 20% was negligible (9).

To resolve this disagreement, we measured elastin's volume as a function of strain and temperature, Fig. 3*A*, and applied the thermodynamic relation $\Delta U = \Delta H - P\Delta V$. Volume was estimated from the digital images of the sample. The coefficients of expansion calculated from the volume data, 14.8×10^{-3} at 15 °C and 3.4×10^{-3} at 38 °C, are in good agreement with previous determinations (10). At temperatures from 10 °C to 45 °C, elastin's volume expands by 5 to 6% when stretched isothermally to a strain of 15%. At 37 °C, the change in internal energy from expansion (−15 ± 2 mJ/g) is small compared to that from enthalpy (−144.5 ± 6.3 mJ/g) and the reduction in internal energy (−159.5 ±mJ/g) is, in fact, large compared to the stretch work (35.5 ± 0.3 mJ/g). As temperature is increased, heat loss is reduced and at 50 °C, the magnitudes of the enthalpy change, and work are comparable (Table 1). Like the effect of temperature, the internal energy loss is also reduced when co-solvents, 0.3 m sodium sulfate or 30% PEG, are added (Fig. 3*C*).

Elastin's volume increases by a large amount, 40%, when cooled (Fig. 3*A*) and we find that the mass and volume of an elastin sample vary in direct proportion with one another (Fig. 3*B*). We conclude that the increase in volume when elastin is stretched or cooled is due entirely to the influx of water, i.e., the changes in the equilibrium volume, dV_{eq}, and the number of moles of water of hydration, dn_{H_2O}, are proportional and related by, $dn_{H_2O} = w_{H_2O}^{-1} dV_{eq}$, where w_{H_2O} is the partial molar volume of water in the elastin matrix. With the known dry mass of the vacuum-dried sample, we find that elastin is 48% and 63% water by weight at 45 °C and 10 °C, respectively.

Cosolvents and Solvent Deuteration Alter Elastin's Mechanical and Thermodynamic Properties. To further confirm the conclusion that the hydrophobic effect is the primary driver of elastic recoil, we have studied elastin's thermomechanics with three cosolvents, Na_2SO_4, 20kD PEG, and $NaClO_4$, and when ^1H_2O is replaced by ^2H_2O, each of which changes water and/or the protein in different ways (Fig. 4). The anions, SO_4^{2-} and ClO_4^-, are strong Hoffmeister ions that are, respectively, kosmotropic and chaotropic, and their effects dominate those from the counterion, Na^+, a weak kosmotrope.

PEG and SO_4^{2-} are widely used to prepare crystalline proteins in their native forms (35). They alter the water:protein interface (36) and increase attractive forces in proteins because they are preferentially excluded from the protein's surface (24, 25, 37). Sulfate increases water's surface tension. This raises the energy required to make the cavity required to accommodate exposed hydrophobic side chains causing the protein to bury hydrophobic residues and become more compact (38). High molecular weight PEG is preferentially excluded from the protein surface because

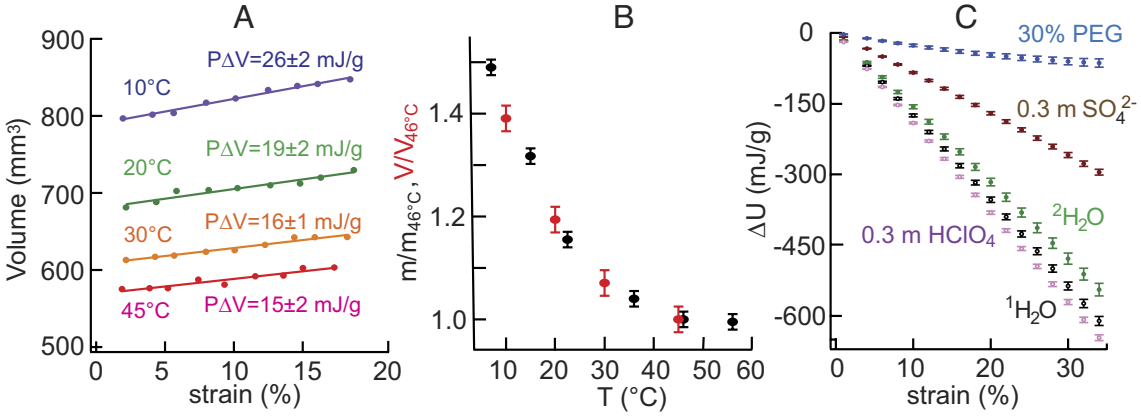

Fig. 3. (*A*) Elastin volume as a function of strain and temperature. Lines are linear fits to the volume vs strain data and the indicated values of $P\Delta V$ are per gram of protein dry weight at 15% strain. (*B*) Temperature dependence of the mass (black) and volume (red) of elastin samples normalized to their values at 46 °C. (*C*) Strain-induced values of ΔU for elastin at 20 °C in the indicated solvents.

Table 1. Thermodynamic properties of elastin recoil from 25% strain in water at three temperatures

property	25 °C	37 °C	50 °C
ΔG, mJ/g	−36.3 ± 0.3	−35.5 ± 0.3	−38.0 ± 0.5
$-T\Delta S$, mJ/g	−360 ± 7	−180 ± 7	−56 ± 19
ΔH, mJ/g	324 ± 7	145 ± 6	18 ± 19
ΔC_p, mJ/g·K	−16.0 ± 0.4	−12.2 ± 0.7	−7 ± 2
ΔU, mJ/g	342 ± 12	160 ± 12	32 ± 21
$P\Delta V$, mJ/g	−18 ± 2	−15 ± 2	−14 ± 2

Sample strain was 25%.

its large size limits penetration into the volume surrounding a protein, known as the exclusion (24, 25) or depletion zone (39). As shown schematically in ref. 39 Fig. 3 and (40), when a protein associates or compacts, the exclusion volume is reduced and the volume available to PEG increases, giving it reduced free energy and greater entropy (39). We find that when Na_2SO_4 or PEG is added at 25 °C, all changes in the thermo-mechanical properties, Fig. 4, are similar to those found in elastin in water when the temperatures is raised above 45 °C, Fig. 2 *E* and *F*. The relaxed length and volume are reduced, the force constant is increased, the entropic force is decreased, the release of heat decreases, the increase in heat capacity is diminished, and the net driving force is nearly unchanged. For example, when elastin is stretched by 25% at 25 °C in 30% PEG, the heat released decreases from 375 mJ/g to 10 mJ/g, *SI Appendix*, Fig. S2, the increase in ΔC_p is reduced from 17 mJ/K to 2 mJ/K, Fig. 4, and the decrease in internal energy equals the stretch work.

Compared to sulfate, elastin is substantially less affected by 0.3 m ClO_4^-, a chaotrope, and changes in l_{rlx} and k_H are in the opposite direction, Fig. 4. Perchlorate binds weakly to the backbone and denatures proteins. When negative charge is added to the nearly neutral elastin matrix, repulsive forces are introduced causing l_{rlx} to increase and k_H to decrease. This effect is small because elastin lacks significant 2° structure (40–43)—weak perchlorate binding to the backbone cannot significantly disrupt a disordered protein. Since 0.3 m ClO_4^- has little effect on surface tension, the large and opposite effects from attractive forces seen with added SO_4^{2-} are absent. However, when the concentration is increased to 1 m, perchlorate becomes kosmotropic with increased surface tension (44) and the changes in l_{rlx} and k_H seen at 0.3 m are reversed (*SI Appendix*, Fig. S1).

When stretched in ^2H_2O, k_H and l_{rlx} are smaller than in ^1H_2O, $T\Delta S$ is less negative, ΔC_p rises faster, and ΔG is unchanged (Fig. 4). Similarly, when folded proteins are denatured in ^2H_2O rather than ^1H_2O, an increase in ΔC_p with constant ΔG (entropy–enthalpy compensation) is usually observed and this has been associated with an increase in solvent-exposed, non-polar surface area (45, 46). These results are fully consistent with the greater solubility of non-polar molecules in ^2H_2O (47) and show that small changes in the strength of the hydrophobic effect have observable effects on the thermodynamics of elastin stretch and recoil. These surface effects are more important than, for example, stronger H-bonds in the protein which should have the opposite effect on the stretch ΔH. This is consistent with our NMR studies indicating a near absence of stable 2° structure in elastin (41, 48) and molecular dynamics simulations of an aggregated elastin-like peptide (11) indicating that putative β—turns stabilized by H-bonds have sub-nanosecond lifetimes. Each of these cosolvents alters the thermodynamics of stretching in elastin in a manner consistent with recoil primarily driven by the hydrophobic effect.

Water Is Ordered when Elastin Is Stretched. The thermodynamic experiments described above provide strong thermodynamic evidence for the primacy of the hydrophobic effect in elastin recoil. We next set out to directly observe water ordering—the hallmark of hydrophobic effect—upon stretching of elastin (29). To determine whether water ordering in elastin varies with strain, we used 2Q filtered ^2H NMR of elastin in ^2H_2O. In this experiment, the signal from bulk water which reorients isotropically is removed and only the 2Q signal from ordered water which reorients anisotropiocally and has a non-zero quadrupole coupling is detected (26, 27). The experiment is quantitated in terms of the water fraction, f_o, that is ordered. Note that elastin's mechanical properties in ^2H_2O are almost the same as in ^1H_2O (Fig. 4). We find that the ordered water fraction, 2% in relaxed elastin, increases substantially to 81% when the sample is stretched by 27% (Fig. 5*A*). This large increase is direct observation of the hydrophobic effect at work during elastin function.

Next, we observed the effects of cosolvent on water ordering: in 10% PEG, the ordered fraction is reduced ~twofold compared to pure ^2H_2O at each stretch (Fig. 5*B*) and further lowered in 0.1 m sodium sulfate (Fig. 5*C*). In 0.5 m sodium sulfate, ordered water is almost eliminated from observation in this experiment (Fig. 5*C*). Overall, these results show that the amount of ordered water decreases with the addition of cosolvents that reduce solvent-exposed surface area: Na_2SO_4 and PEG.

Discussion

To understand the molecular basis of recoil in elastin, we have combined a complete study of elastin's thermodynamics and measured water ordering in the elastin matrix at the molecular level. Under physiological conditions, elastin is a non-ideal elastomer, as summarized in Table 1. At 37 °C, the entropic force that drives recoil, $-T\Delta S$, is fivefold greater than the magnitude of the net driving force, ΔG. In rubber, the entropic and the net driving force are approximately equal, as is the case for an ideal elastomer (22). Because $-T\Delta S$ and the enthalpy change, ΔH, are opposed (opposite sign), elastin has high compliance. Otherwise, a heart with greater contractive force would be required to expand arteries. From Le Chatelier's principle, the large heat absorption with recoil follows directly from the large decrease in the relaxed length when the temperature is raised (Fig. 1*D*). At 50 °C, the relaxed length reaches a constant value. Consequently, ΔH and $T\Delta S$ for recoil from 25% strain are drastically reduced to 18.1 ± 19 mJ/g and 56.3 ± 19 mJ/g, respectively, from their values at 5 °C, 760 ± 19 mJ/g and 801 ± 19 mJ/g. Since ΔG is nearly constant, −38.0 ± 0.5 mJ/g at 50 °C and −41.5 ± 0.5 mJ/g at 5 °C, there is significant enthalpy–entropy compensation. This and the stretch-induced increase in the heat capacity, also observed here, are signature features of the hydrophobic effect.

With thermomechanics, we have confirmed that the heat released from stretch is in large excess over the total work performed, previously determined using a calorimeter (4, 9). In addition, we have determined that this process is fully reversible (Fig. 1*C*). Thus, objections to this finding based on a time-scale argument (5) can be disregarded. Because ΔH from stretch is large and negative, Weis-Fogh concluded that, unlike rubber (22), elastin's internal energy had decreased. Flory, however, observed no change in the volume or internal energy when elastin was stretched in 30% PEG and concluded that elastin is like rubber (2). While Weis-Fogh had assumed that volume was constant when stretched,

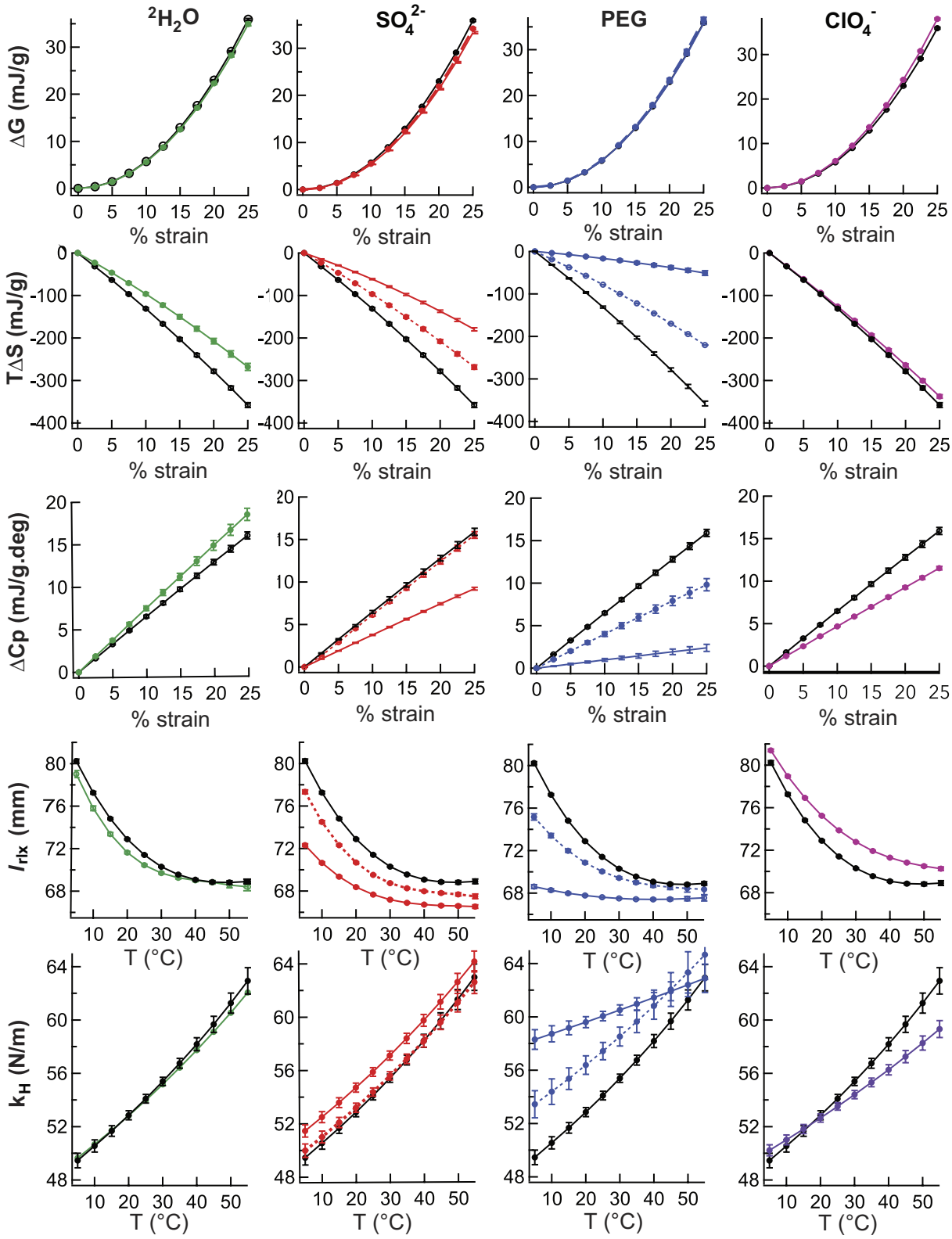

Fig. 4. Thermomechanical properties of elastin in different aqueous solutions. Columns in the figure are the different solvents: ^2H_2O (green), Na_2SO (···0.1 m and −0.3 m, red), 20 kDa PEG (···15% and −30%, blue), and $NaClO_4$ (– 0.3 m, purple). Rows in the figure are thermodynamic parameters (ΔG, TΔS, and ΔC_p) are plotted vs. % strain at 25 °C and the mechanical parameters (l_{rlx} and k_H) are plotted vs. temperature. For reference, the data from elastin in pure water (black) are shown in each graph.

Flory had assumed that PEG has negligible effect on water:protein interactions. To resolve this, we have measured elastin's volume as a function of temperature and strain and used the general relation, $\Delta U = \Delta H - P\Delta V$, to determine ΔU in pure water and in 30% PEG. We concur that ΔV in 30% PEG is negligible, however, ΔV is small in water and the contribution to the internal energy is less than 10% of ΔH (Figs. 2 and 3). Thus, in physiological conditions, ΔU decreases when elastin is stretched. The difference between elastin in water and 30% PEG is primarily the difference in ΔH and not ΔV.

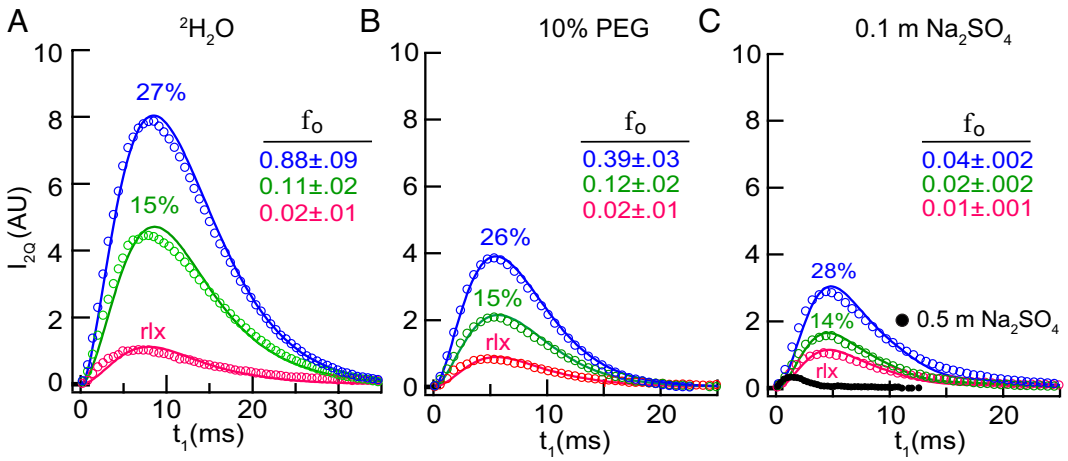

Fig. 5. Plots of the deuterium 2Q NMR signal intensity, I_{2Q}, as a function of the 2Q preparation time, t_1. Open circles are the intensities of the 2Q-filtered NMR signal with only every third data point shown. The ordered fraction, f_o, was determined by least-squares fitting (solid lines) to Eq. **18**. Elastin fibers were hydrated in (*A*) ^2H_2O, (*B*) 10% PEG (w/w), (*C*) 0.1 m Na_2SO_4, and 0.5 m Na_2SO_4 at 28% stretch (black dots). The fibers are relaxed (red), 14 to 15% stretched (green), and 26 to 28% stretched (purple).

To better understand the effects of cosolvents, we have determined elastin's thermo-mechanical properties and the ordered water fraction, f_o, with three cosolvents. Sodium sulfate and PEG change the water:protein interface, do not bind to the protein and promote protein compaction while perchlorate binds to the protein, has little effect on water properties, and leads to protein expansion. These expectations are fully borne out in changes to elastin's thermo-mechanical properties (Fig. 4) and to changes in the ordered water fraction, f_o (Fig. 5). The relaxed length decreases by a large amount in sulfate or PEG and increases by a small amount in perchlorate. ΔG is essentially unchanged by any of the co-solvents while the magnitudes of $T\Delta S$, ΔH, and ΔC_p are all significantly and progressively decreased by large amounts in sulfate and PEG but almost unchanged in 0.3 m perchlorate. In 30% PEG, ΔH and ΔC_p approach zero, $\Delta G \sim -T\Delta S$ (*SI Appendix*, Fig. S2), and the ordered water fraction in the NMR experiment is greatly reduced.

Conclusions

At physiological temperature, recoil in elastin is characterized by several unusual properties: i) the internal energy increases, ii) the heat capacity decreases, iii) the entropic driving force is large compared to the net driving force because spontaneous recoil is highly endothermic, and iv) stretching elastin orders water. Properties (ii), (iii), and (iv) are characteristic of a spontaneous process driven by the hydrophobic effect (29, 30) and all of these properties are different or absent in rubber where the driving force for recoil is the increase in the polymer's configurational entropy (21, 49). We conclude that at physiological temperatures and in the absence of cosolvents, the predominant driving force for recoil in elastin is the hydrophobic effect.

Natural and artificial configurational entropy springs such as rubber suffer from strain crystallization while experiencing repeated strain cycles, undergoing microscopic phase transitions that result in zones of ordered material with low compliance (50). Hydrophobic effect-driven recoil may be the origin of elastin's unusual resilience in that it offers a pathway to avoid these phase transitions by retaining disorder even while extended, enabling elastin to be less prone to hysteresis than rubber because water reorientation is more facile than chain motion in a condensed polymer.

Materials and Methods

Thermodynamic Properties from the Temperature Dependence of Elastin's Mechanical Properties. At constant temperature and pressure, elastin immersed in water is an open system in equilibrium with the surrounding solvent and the relevant thermodynamic expression is the Gibbs free energy (29),

$$dG = -SdT + VdP + Fdl + \mu dn. \quad [1]$$

In Eq. **1**, F is force, l is the sample length and, respectively, n and μ are the number of moles and chemical potential of water in the elastin matrix. The chemical potential term, μdn, accounts for a change in hydration of the elastin matrix when it is stretched or the temperature is changed. Other variables have their usual meaning. It is shown in Fig. 3*C*, and the related discussion, that when elastin is at osmotic equilibrium (*eq*) with the surrounding water, the changes in elastin's volume and moles of water are related by, $dn_{H_2O} = w_{H_2O}^{-1} dV_{eq}$, where w_{H2O} is the partial molar volume of water in the elastin matrix. Since V_{eq} depends only on temperature and length, dV_{eq} can be expanded in dT and dl,

$$dn = \frac{\left(\partial V_{eq}/\partial T\right)_l dT + \left(\partial V_{eq}/\partial l\right)_T dl}{w_{H_2O}}. \quad [2]$$

Substituting Eq. **2** into Eq. **1** gives a free energy expression subject to the constraint that hydrated elastin is at equilibrium with the water in which it is immersed.

$$dG = -\left(S - \mu/w_{H_2O}\left(\partial V_{eq}/\partial T\right)_l\right)dT + V_{eq}dp + \left(F + \mu/w_{H_2O}\left(\partial V_{eq}/\partial l\right)_T\right)dl. \quad [3]$$

From Eq. **3**, the following Maxwell relation (51) is obtained:

$$\left(\partial S/\partial l\right)_{T,P,eq} = -\left(\partial F/\partial T\right)_{l,P,eq}. \quad [4]$$

Terms containing V_{eq} cancel because the order of partial differentiation does not matter. After Eq. **4** is integrated with respect to l, the relation for the entropy change is

$$\Delta S_{T,P,eq} = -\int \left(\partial F(l,T)/\partial T\right)_{l,P,eq} dl. \quad [5]$$

Because the volume change with stretch is small, Fig. 3*A* and $\left(\partial V_{eq}/\partial l\right)_T < 4$ mm^2, $\Delta G_{T,P,eq}$ is the integral of the stretch force with respect to l,

$$\Delta G_{T,P,eq} = \int F(l,T)dl. \quad [6]$$

Previously, Flory separated the total strain (f = F/a and a = the cross-sectional area) into the sum, respectively, of enthalpic (f_H) and entropic (f_S) components, (13)

$$f = \left(\partial H/\partial l\right)_{T,P,n} + T\left(\partial f/\partial T\right)_{l,P,n}. \quad [7]$$

It is shown, in the *SI Appendix*, that Eq. **7** for a system in equilibrium with the surrounding solvent can be derived directly from Eqs. **4** and **6** and the definition of the Gibbs free energy.

To experimentally determine $F(l, T)$, the sample length, l, was measured from 3 °C to 55 °C with forces from 0.09 N to 0.72 N at each temperature. The length was found to accurately fit a virial equation of state that is 1st-order in $\tilde{F} \equiv F - \overline{F}$ and 3rd-order in $\tilde{T} \equiv T - \overline{T}$.

$$l(\tilde{F},\tilde{T}) = b_{00} + b_{10}\tilde{F} + b_{01}\tilde{T} + b_{11}\tilde{F}\tilde{T} + b_{02}\tilde{T}^2 + b_{03}\tilde{T}^3. \quad [8]$$

The polynomial, Eq. **8**, is an expansion about the averages of the experimental forces and temperatures, $\overline{F}$ and $\overline{T}$. The coefficient b_{12} was found to be zero within experimental error and not included in Eq. **8**. With the definitions of the length at zero force,

$$l_{rlx} \equiv b_{00} + b_{01}\tilde{T} + b_{02}\tilde{T}^2 + b_{03}\tilde{T}^3 - \left(b_{10} + b_{11}\tilde{T}\right)\overline{F}, \quad [9]$$

and the spring constant,

$$k_H \equiv (b_{10} + b_{11}\tilde{T})^{-1}, \quad [10]$$

Eq. **8** can be solved for F and written in the form of Hooke's law,

$$F = k_H(l - l_{rlx}). \quad [11]$$

Note that k_H and l_{rlx} are temperature-dependent functions of the virial coefficients and are related to the Young's modulus by $E = k_H l_{rlx}/a$. They provide greater physical insight than the Young's modulus alone and all thermodynamic properties can be calculated from them. The free energy (non-$P\Delta V$ work) is obtained by inserting Eq. **11** into Eq. **6** and integrating,

$$\Delta G_{T,P,eq} = \frac{1}{2}k_H\Delta l^2, \quad [12]$$

and $\Delta l \equiv l - l_{rlx}$. Differentiating Eq. **11** with respect to temperature, we obtain,

$$\left(\partial F/\partial T\right)_l = \left(l - l_{rlx}\right)\left(\partial k_H/\partial T\right)_l - k_H\left(\partial l_{rlx}/\partial T\right)_l, \quad [13]$$

which is inserted into Eq. **5** and integrated to obtain the entropy change,

$$\Delta S_{T,P,eq} = -\frac{1}{2}\left(\frac{\partial k_H}{\partial T}\right)_l \Delta l^2 + k_H\left(\frac{\partial l_{rlx}}{\partial T}\right)_l \Delta l. \quad [14]$$

In turn, $\Delta H_{T,P,eq}$, is obtained using the general expression $\Delta H = \Delta G + T\Delta S$ and the heat capacity, $\Delta C_p = (\partial \Delta H_{T,P,eq}/\partial T)_P$, is:

$$\Delta C_p = \left(\frac{\partial \Delta G}{\partial T}\right)_P + T\left(\frac{\partial \Delta S}{\partial T}\right)_P + \Delta S. \quad [15]$$

The partial derivatives in Eq. **15** are obtained from Eqs. **12** and **14** yielding,

$$\Delta C_p = -\frac{1}{2}\tilde{T}\left(\frac{\partial^2 k_H}{\partial T^2}\right)_l \Delta l^2 + \left[k_H\tilde{T}\left(\frac{\partial^2 l_{rlx}}{\partial T^2}\right)_l + k_H\left(\frac{\partial l_{rlx}}{\partial T}\right)_l + \tilde{T}\left(\frac{\partial l_{rlx}}{\partial T}\right)_l\left(\frac{\partial k_H}{\partial T}\right)_l\right]\Delta l. \quad [16]$$

Analytical expressions for the partial derivatives in Eqs. **14** and **16** are readily obtained from the definitions of l_{rlx} *and* k_H, Eqs. **9** and **10**.

$$\left(\frac{\partial k_H}{\partial T}\right)_l = -k_H^2 b_{11}, \quad [17]$$

$$\left(\frac{\partial l_{rlx}}{\partial T}\right)_l = b_{01} + 2b_{02}\tilde{T} + 3b_{03}\tilde{T}^2 - b_{11}\overline{F}, \quad [18]$$

$$\left(\frac{\partial^2 k_H}{\partial T^2}\right)_l = 2b_{11}^2 k_H^3, \quad [19]$$

$$\left(\frac{\partial^2 l_{rlx}}{\partial T^2}\right) = 2b_{02} + 6b_{03}\tilde{T}. \quad [20]$$

Elastin Sample Preparation. A 0.24 g dried elastin fiber (~ 77 mm × 1.6 mm × 6.4 mm) was cut from purified, bovine neck ligament. The purification procedure (32), avoids harsh conditions used in older procedures, removes microfibrils and collagen and preserves fibrillar structure of native elastin (Fig. 1*A*). A single sample was used for all of the thermo-mechanical data reported in Table 1 and Figs. 1–4. After each co-solvent study, the sample was back exchanged into water and a length vs. temperature curve (*SI Appendix*, Fig. S6) confirmed that the cosolvent had been removed and the sample was unchanged. The sample was glued (Elmer's E616 Super Glue) to 1/4″ diameter rods at both ends for attachment to the stretcher apparatus. A separate and larger sample was used to determine the temperature dependence of elastin's mass (Figure 6b). With the larger sample (dry mass of 2.029 g), the contribution to the total mass from water on the surface of the sample was minimized. After removal from the temperature-controlled water bath, samples were quickly blotted on a chem-wipe before weighing. Additional water loss that occurs on sample warming was minimized by performing the experiments in the cold room.

Stretcher Instrument. The sample compartment of the apparatus (*SI Appendix*, Fig. S4) used to determine $F(l, T)$ and $V(l, T)$ was machined from delrin (sides and base) and plexiglass windows (front and back) through which the fiber was photographed with a 36-megapixel digital camera (Sony A7r). The short rod glued to the lower end of the elastin sample was fixed to the base and the top rod was attached to a string that was passed over a low friction pulley (Super pulley, ME9450a, Pasco, Roseville, CA) to an adjustable mass that was converted to force using the acceleration due to gravity, 9.8 m/s^2. The camera and tank were rigidly fixed to a table, from which the fiber length was measured as a function of applied force and temperature with an accuracy of 0.1 mm to 0.2 mm using ImageJ software (https://imagej.nih.gov/ij/). The digital image was calibrated against a 200 mm ruler placed next to the sample. The temperature controller (blue box in *SI Appendix*, Fig. S4*C*) regulated to within 0.1 °C of the set point with a PID controller and the temperature was measured with a platinum resistance thermometer placed in the sample compartment. To avoid thermal gradients, solvent was continuously circulated from the top to the bottom of the tank by a miniature pump.

Volume as a Function of Strain and Temperature. The sample volume was determined directly from the digital image. Combined with the length measurement, the sample width along the length of the elastin sample was also measured and the sample thickness, the smallest dimension, was calculated from the width measurement with the assumption that the thickness to the width ratio was the same as in the dry sample.

Thermo-Mechanical Data Collection, Analysis, and SE Determinations. Length vs. force and temperature data were collected as separate $l(F)$ runs at 9 forces from 0.09N to 0.72N and $l(T)$ runs collected at 1 °C intervals from 2 °C to 55 °C. The data were combined into a single table with a typical size of 300 $l(F, T)$ values from which thermo-mechanical properties were calculated using the two Matlab scripts listed in *SI Appendix*. With the first script, the $F(l, T)$ data were least-squares fit to Eq. **8** to determine the virial coefficients, b_{ij}, from which all thermo-mechanical properties were calculated in the second script using Eqs. **9**–**20**.

SE were determined by propagating the effects of random errors in a) the experimental lengths, l, or b) the virial coefficients, b_{ij}, into the thermo-mechanical properties (33). Errors in l were simulated by adding a random error to each experimental value of l sampled from a normal distribution with a SD equal to the accuracy of the measurements in our experimental apparatus, 0.25 mm. Multiple datasets simulated in this way were each fit to Eq. **8**, from which a distribution of values was calculated for each thermo-mechanical properties as a function of

strain and temperature using Eqs. **9**–**20**. Alternatively, random errors were added to the coefficients, b_{ij}, using the SE, σ_{ij}, from the fit of the experimental data to Eq. **8** and *SI Appendix*, Table S1, and distributions of properties were calculated as in (a). SD of the distributions converged with 1,000 simulations and are used as SE for all properties. To avoid over interpreting the results, the twofold larger SE obtained with method (b) have been used throughout and are shown as error bars at the regular intervals in Figs. 2 and 4 and *SI Appendix*, Figs. S1–S3. SE in Table 1 were calculated in the same way.

Strain Induced Changes in Solvent Ordering Studied by 2Q ^{2}H NMR. We have observed the effect of stretch on ordering of ^2H_2O in the elastin matrix. Insofar as molecular reorientation of ^2H_2O is anisotropic, as is the case for ordered water, ^2H_2O has a non-zero ^{2}H quadrupole coupling and the "forbidden" 2Q NMR transition can be observed using the methods of indirect detection. (28) Because reorientation in bulk water is isotropic, the quadrupole coupling is averaged to zero, the 2Q transition is absent and its NMR signal can be removed by 2Q filtration and only the 2Q transition is observed (26, 27). To determine the effect of strain on the fraction of ordered water in the sample, f_o, we observed the buildup of the 2Q NMR signal from ordered water, I_{2q}, as a function of the 2Q preparation time, t_1. The NMR signal is proportional to f_o and is well-described by the relation (26),

$$\frac{I_{2q}\left(t_1\right)}{I_{1Q}^{tot}} = f_o e^{-2R_2 t_1}\int_0^{\pi} sin^2\left[\frac{\omega_0 t_1}{2}\left(3cos^2\theta - 1\right)\right] sin\theta d\theta. \quad [\mathbf{21}]$$

The ordered fraction, f_o, and the residual quadrupole coupling, $\nu_Q = \omega_Q/2\pi$, were determined by a two parameter least-squares fit of $I_{2q}(t_1)$ to equation **21** with I_{1Q}^{tot}, the 1Q signal from all of the ^2H_2O in the sample, and R_2, the transverse relaxation time, constrained to the values separately determined in Hahn echo experiments with and without 2Q filtration (*SI Appendix*, Fig. S5) (26).

2Q filtered ^{2}H spectra were collected on a homebuilt, 11.6 T instrument with a solenoidal coil probe (52) (90° pulse width = 4.2 μs) and the previously described pulse sequence and phase cycle (26). ^{2}H spectra (2k complex points) were obtained with a 4 or 5 kHz offset and 128 equally spaced 2Q preparation times, t_1. Two-dimensional spectra were Fourier transformed in the observed dimension, t_2, and peak heights of the 2Q filtered signals are displayed (Fig. 5) as a function of the 2Q preparation time, t_1. Suppression of the 1Q signal from bulk water to a level below the noise was confirmed in two ways. All NMR signals in Fig. 5 at zero 2Q preparation times ($t_1 = 0$) are, within the S/N ratio of the experiments, also zero and 1Q bulk water signals would have been observed only if 2Q filtration was insufficient, as was not the case. In the 2D spectrum, *SI Appendix*, Fig. S6, the 1Q (bulk water) and 2Q (ordered water) signals are separated in the F_1 dimension and the phase cycle for eliminating the bulk water (1Q) signal is applied (26). With a 4 kHz offset, the ordered water peak at $F_1 = 8$ kHz is large (S/N = 47:1) and the bulk water peak at $F_1 = 4$ kHz, is reduced to below the noise level. Furthermore, in each of the graphs shown in Fig. 5, the 2Q signal at short 2Q preparation times is below the noise level and this is only possible if the much larger bulk water signal is adequately suppressed by the phase cycle.

NMR Sample Preparation. Both ends of a purified elastin fiber (~20 mg and ~1 mm × ~12 mm) were superglued to ~12 mm lengths of 1/16″ diameter plastic rod, equilibrated overnight in the desired aqueous solution and inserted into a 3 mm NMR tube (length ~30 mm) after removal of excess solvent by blotting on paper. With the elastin sample centered in the NMR tube, one rod was sealed and held stationary to the tube with glue and the other rod was sealed and held in place with parafilm which could be removed so that the fiber could be stretched to a different length and resealed. Fiber lengths were measured with a digital caliper.

Materials. Elastin samples were purified from fresh bovine nuchae membranes using a method that preserves the natural fibrous structure and removes other proteins (Fig. 1*A*) (32). Elastin was washed in aqueous sodium chloride for 3 d to remove soluble proteins followed by ethanol, chloroform, methanol, and acetone extraction to remove lipids. Because elastin has no methionine residues and the ε-amino groups of lysyl residues are oxidized for cross-linking, remaining proteins were removed by washing after proteolysis with cyanogen bromide and trypsin. This material has nearly the same modulus at 24 °C as was measured in unpurified, single elastin fibers (53). Dry fibers were stored at −80 °C. Sample solutions were prepared from deionized water with reagent-grade solutes (Na_2SO_4, 20 kDa PEG, and $NaClO_4$). The experiments in deuterated solvent used 99% ^2H_2O (Cambridge Isotopes, Andover, MA).

Data, Materials, and Software Availability. The custom Matlab scripts used to calculate the virial coefficients from the raw thermodynamic data and the thermomechanical properties and their associated CI from the virial coefficients are in the *SI Appendix*. Data is deposited at https://academicworks.cuny.edu/cc_pubs/985/ (54). All thermomechanical data have been distilled into the virial coefficients listed in *SI Appendix*, Table S1, from which properties in Figs. 2, 3*C*, and 4 were calculated as described in the *Materials and Methods* sections.

ACKNOWLEDGMENTS. The authors gratefully acknowledge support from the NSF (DMR-1410678) to R.L.K. and R.J.W. and help in fitting the NMR data from Dr. Abed Jamhawi.

1. L. Robert, A. M. Robert, T. Fulop, Rapid increase in human life expectancy: Will it soon be limited by the aging of elastin? *Biogerontology* **9**, 119–133 (2008).
2. C. A. Hoeve, P. J. Flory, The elastic properties of elastin. *Biopolymers* **13**, 677–686 (1974).
3. C. A. J. Hoeve, P. J. Flory, The elastic properties of elastin 1,2. *J. Am. Chem. Soc.* **80**, 6523–6526 (1958).
4. T. Weis-Fogh, S. O. Anderson, New molecular model for the long-range elasticity of elastin. *Nature* **227**, 718–721 (1970).
5. K. Dorrington, W. Grut, N. G. McCrum, Mechanical state of elastin. *Nature* **255**, 476–478 (1975).
6. K. L. Dorrington, N. G. McCrum, Elastin as a rubber. *Biopolymers* **16**, 1201–1222 (1977).
7. W. Grut, N. G. McCrum, Liquid drop model of elastin. *Nature* **251**, 165–165 (1974).
8. B. B. Aaron, J. M. Gosline, Elastin as a random-network elastomer–A mechanical and optical analysis of single elastin fibers. *Biopolymers* **20**, 1247–1260 (1981).
9. J. M. Gosline, Hydrophobic interaction and a model for the elasticity of elastin. *Biopolymers* **17**, 677–695 (1978).
10. J. M. Gosline, Temperature-dependent swelling of elastin. *Biopolymers* **17**, 697–707 (1978).
11. S. Rauscher, R. Pomes, The liquid structure of elastin. *Elife* **6**, e26526 (2017).
12. B. Li, D. O. V. Alonso, B. J. Bennion, V. Daggett, Hydrophobic hydration is an important source of elasticity in elastin-based biopolymers. *J. Am. Chem. Soc.* **123**, 11991–11998 (2001).
13. C. A. J. Hoeve, P. J. Flory, Elasticity of crosslinked amorphous polymers in swelling equilibrium with diluents. *J. Polymer Sci.* **60**, 155 (1962).
14. V. Samouillan, C. Andre, J. Dandurand, C. Lacabanne, Effect of water on the molecular mobility of elastin. *Biomacromolecules* **5**, 958–964 (2004).
15. M. S. Paterson, Effect of pressure on Young's modulus and the glass transition in rubbers. *J. Appl. Phys.* **35**, 176–179 (1964).
16. A. J. Cocciolone *et al.*, Elastin, arterial mechanics, and cardiovascular disease. *Am. J. Physiol. Heart Circ. Physiol.* **315**, H189–H205 (2018).
17. B. Vrhovski, A. S. Weiss, Biochemistry of tropoelastin. *Eur. J. Biochem.* **258**, 1–18 (1998).
18. A. Vidal Ceballos *et al.*, Liquid to solid transition of elastin condensates. *Proc. Natl. Acad. Sci. U.S.A.* **119**, e2202240119 (2022).
19. D. He *et al.*, Comparative genomics of elastin: Sequence analysis of a highly repetitive protein. *Matrix Biol.* **26**, 524–540 (2007).
20. T. A. Weis-Fogh, S. O. Anderson, New molecular model for the long-range elasticity of elastin. *Nature* **227**, 718–721 (1970).
21. M. C. Shen, D. A. McQuarrie, J. L. Jackson, Thermoelastic behavior of natural rubber. *J. Appl. Phys.* **38**, 791–798 (1967).
22. L. R. G. Treloar, *The Physics of Rubber Elasticity* (Clarendon Press, Oxford, ed. 3, 1975).
23. J. M. Gosline, The elastic properties of rubber-like proteins and highly extensible tissues. *Symp. Soc. Exp. Biol.* **34**, 332–357 (1980).
24. T. Arakawa, S. N. Timasheff, Mechanism of poly(ethylene glycol) interaction with proteins. *Biochemistry* **24**, 6756–6762 (1985).
25. R. Bhat, S. N. Timasheff, Steric exclusion is the principal source of the preferential hydration of proteins in the presence of polyethylene glycols. *Protein Sci.* **1**, 1133–1143 (1992).
26. T. V. Krivokhizhina, R. Wittebort, 2Q NMR of ^2H_2O ordering at solid interfaces. *J. Magn. Res.* **243**, 33–39 (2014).
27. T. Meersmann, S. A. Smith, G. Bodenhausen, Multiple-quantum filtered xenon-131 NMR as a surface probe. *Phys. Rev. Lett.* **80**, 1398–1401 (1998).
28. R. R. Ernst, G. Bodenhausen, A. Wokaun, *Principles of Nuclear Magnetic Resonance in One and Two Dimensions* (Oxford University Press, London/New York, 1987).
29. K. A. Dill, S. Bromberg, D. Stigter, *Molecular Driving Forces, Statistical Thermodynamics in Biology, Chemistry, Physics, and Nanoscience* (Taylor & Francis Group, ed. 2, 2003).
30. K. R. Gallagher, K. A. Sharp, A new angle on heat capacity changes in hydrophobic solvation. *J. Am. Chem. Soc.* **125**, 9853–9860 (2003).
31. K. A. Sharp, B. Madan, Hydrophobic effect, water structure, and heat capacity changes. *J. Phys. Chem. B* **101**, 4343–4348 (1997).
32. W. F. Daamen, T. Hafmans, J. H. Veerkamp, T. H. van Kuppevelt, Isolation of intact elastin fibers devoid of microfibrils. *Tissue Eng.* **11**, 1168–1176 (2005).
33. W. H. Press, S. A. Teukolsky, W. T. Vetterling, *Numerical Recipes in Fortran 77, volume 1: The Art of Scientific Computing* (Cambridge University Press, 1992).
34. C. Tanford, *The Hydrophobic Effect: Formation of Micelles and Biological Membranes* (J. Wiley, New York, 1973).
35. A. McPherson, J. A. Gavira, Introduction to protein crystallization. *Acta Crystallogr.F Struct. Biol. Commun.* **70**, 2–20 (2014).

36. L. M. Pegram, M. T. Record Jr., Quantifying accumulation or exclusion of H(+), HO(-), and Hofmeister salt ions near interfaces *Chem. Phys. Lett.* **467**, 1–8 (2008).
37. S. N. Timasheff, T. Arakawa, Mechanism of protein precipitation and stabilization by co-solvents. *J. Crystal Growth* **90**, 39–46 (1988).
38. T. Y. Lin, S. N. Timasheff, On the role of surface tension in the stabilization of globular proteins. *Protein Sci.* **5**, 372–381 (1996).
39. S. Finet, D. Vivares, F. Bonnete, A. Tardieu, "Controlling biomolecular crystallization by understanding the distinct effects of PEGs and salts on solubility" in *Macromolecular Crystallography*, C. W. Carter, R. M. Sweet, Eds. (Elsevier, 2003), vol. 368, pp. 105–129.
40. K. N. Greenland *et al.*, Order, disorder, and temperature-driven compaction in a designed elastin protein. *J. Phys. Chem. B* **122**, 2725–2736 (2018).
41. M. Carvajal *et al.*, Dynamics in natural and designed elastins and their relation to elastic fiber structure and recoil. *Biophys. J.* **120**, 4623–4634 (2021).
42. S. E. Reichheld, L. D. Muiznieks, F. W. Keeley, S. Sharpe, Direct observation of structure and dynamics during phase separation of an elastomeric protein. *Proc. Natl. Acad. Sci. U.S.A.* **114**, E4408–E4415 (2017).
43. C. U. Schrader *et al.*, Elastin is heterogeneously cross-linked. *J. Biol. Chem.* **293**, 15107–15119 (2018).
44. Y. Cho *et al.*, Effects of hofmeister anions on the phase transition temperature of elastin-like polypeptides. *J. Phys. Chem. B* **112**, 13765–13771 (2008).
45. M. M. Lopez, G. I. Makhatadze, Solvent isotope effect on thermodynamics of hydration. *Biophys. Chem.* **74**, 117–125 (1998).
46. G. I. Makhatadze, G. M. Clore, A. M. Gronenborn, Solvent isotope effect and protein stability. *Nat. Struct. Biol.* **2**, 852–855 (1995).
47. Y. Marcus, A. Bennaim, A study of the structure of water and its dependence on solutes, based on the isotope effects on solvation thermodynamics in water. *J. Chem. Phys.* **83**, 4744–4759 (1985).
48. M. S. Pometun, E. Y. Chekmenev, R. J. Wittebort, Quantitative observation of backbone disorder in native elastin. *J. Biol. Chem.* **279**, 7982–7987 (2004).
49. D. N. Simavilla, J. D. Schieber, D. C. Venerus, Evidence of deformation-dependent heat capacity and energetic elasticity in a cross-linked elastomer subjected to uniaxial elongation. *Macromolecules* **51**, 589–597 (2018).
50. P.-A. Albouy, P. Sotta, Strain-induced crystallization in natural rubber. *Polym. Cryst. II* **277**, 167–205 (2015).
51. D. A. McQuarrie, J. D. Simon, *Physical Chemistry: A Molecular Approach* (University Science Books, Sausalito, CA, 1997).
52. Q. W. Zhang *et al.*, Double and triple resonance circuits for high-frequency probes. *J. Magn. Res.* **132**, 167–171 (1998).
53. B. B. Aaron, J. M. Gosline, Optical-properties of single elastin fibers indicate random protein conformation. *Nature* **287**, 865 (1980).
54. N. M. Jamhawi, R. L. Koder, R. J. Wittebort, Raw Data files for the manuscript "Elastin Recoil is Driven by the Hydrophobic Effect." Publications and Research. https://academicworks.cuny.edu/cc_pubs/985/. Deposited 1 August 2023.